



Unravelling the photocatalytic degradation of polyethylene microplastics with TiO₂ under UV light: Evidence from kinetic studies*

Daniel Aragón, Carmen Barquín, Eugenio Bringas, Inmaculada Ortiz, María J. Rivero*

Departamento de Ingenierías Química y Biomolecular, ETSIIT, Universidad de Cantabria, Avda. Los Castros s/n, 39005 Santander, Spain



ARTICLE INFO

Keywords:
Microplastics
Photocatalysis
Degradation
Polyethylene
TiO₂

ABSTRACT

The accumulation of plastic debris in water bodies requires urgent remediation. Significant research efforts are being made for the effective capture of microplastics (MPs), but a technology to achieve the complete degradation is still a must. Photocatalysis of MPs mediated by the action of semiconductor materials under light irradiation deserves attention due to its advantageous environmental and energetic characteristics. Here, we aim to contribute to this field by a detailed experimental analysis of the photocatalytic degradation of polyethylene (PE) microspheres, selected as target MPs, with TiO₂ P25 as the photocatalyst. Dark and photolysis experiments do not achieve significant degradation yields. Additionally, under the experimental conditions and after 8 h of treatment the photocatalytic degradation is evidenced by: i) gravimetric analysis that resulted in a 34.0 ± 1.4 % of mass loss, ii) chemical transformation quantified through a 58.5 % increase in the carbonyl index, and iii) particle size reduction, from an initial size of 234 ± 12 µm to an average diameter of 185 ± 13 µm. Furthermore, changes in the dissolved organic carbon, detection of short-chain acids in solution and CO₂ in the gas phase, confirm the degradation of the initial MPs. It is noteworthy that the implementation of consecutive cycles contributes to increase the degradation yield, increasing the mass loss to 54 % after 5 cycles. Photocatalysis phytotoxicity analysis in different water matrices demonstrates that treated water is suitable for irrigation. This research represents a step forward in the analysis of the photocatalytic degradation of MPs in water.

1. Introduction

The extensive production and application of polymers in recent decades has led to the generation of considerable amounts of plastic waste, which has adversely impacted the environment [1]. Plastic particles with diameters lower than 5 mm are considered MPs and have been identified as an emerging threat due to their high lifetime, lack of biodegradability and their ability to enter biotic species, including humans, through ingestion and inhalation, causing a serious threat to the health of living beings [2,3]. MPs are classified into primary and secondary ones, depending on the sources from which they are generated [4]. Primary MPs are widely used in granular materials, cosmetics and other personal care products, including toothpaste and scrubs [5]. Secondary MPs result from the fragmentation and deterioration of larger plastics in terrestrial and aquatic environments as they can be exposed to aggressive agents and small fragments are broken off from the original material through tearing, friction or mechanical means [6,7].

In recent years, concern over MPs has risen steadily. Despite the

recent enactment of legislation prohibiting single-use MPs and plastics in the European Directive 2019/904 [8], these contaminants continue to be present in the environment, primarily as a result of secondary sources [9,10], being water bodies one of the main reservoirs of MPs. Researches, such as Okoffo et al. [11] reported that raw influents of three wastewater treatment plants (WWTPs) in Australia exhibited concentrations of 3116, 1811 and 840 µg L⁻¹ of plastics. Moreover, microplastics with sizes below 100 µm were also identified in surface water in Czech Republic with concentrations ranging from 4464 particles L⁻¹ to 3065 particles L⁻¹ [12], and Xu et al. [13] identified in China concentrations between 0.283–0.793 µg L⁻¹ and 0.021–0.203 µg L⁻¹ in surface water and groundwater, respectively. That presence has the potential to induce severe toxicological consequences, resulting in organ damage to humans and other organisms [14]. Furthermore, their hydrophobicity and relatively high specific surface area render them capable of adsorbing other contaminants, thus providing a vector for the transportation of other persistent organic pollutants. The accumulation of MPs in the environment, coupled with their potential hazardous effects,

* This article is part of a Special issue entitled: 'AOT_Innovation' published in Chemical Engineering Journal.

* Corresponding author.

E-mail address: [\(M.J. Rivero\).](mailto:marijose.rivero@unican.es)

has led to an urgent need to develop effective removal methods. However, only a limited number of researches have reported its removal from aqueous media [15,16]. Furthermore, the new European Directive 2024/3019 [17], concerning urban wastewater, points out that quaternary treatment should be introduced in order to ensure that a wide range of the remaining micropollutants is removed from urban wastewater. Consequently, it can be deduced that the development of economically viable and efficient alternatives to remove these pollutants from water is imperative.

Advanced Oxidation Processes (AOPs) have been demonstrated to be effective in the decontamination of water containing organic pollutants. They are mainly based on the production of reactive oxygen species capable of oxidizing and mineralizing even the most recalcitrant molecules, resulting in carbon dioxide (CO_2) and inorganic ions [18,19]. Heterogeneous photocatalysis is a sustainable and environmentally friendly technique to break the molecules of organic contaminants and form H_2O and CO_2 . In that technology, light is utilized to photo-excite a semiconductor catalyst in the presence of oxygen. Semiconductors, such as titanium dioxide (TiO_2), zinc oxide (ZnO), and cadmium sulfide (CdS), can act as catalysts for light-induced redox processes due to their electronic structure, which is characterized by a filled valence band and an empty conduction band. The absorption of a photon with an energy greater than the bandgap energy results in the formation of an electron-hole pair. The degradation of organic contaminants can be achieved through the formation of radicals from photoexcited electrons or photoinduced holes, or by direct oxidation of the catalyst surface by electrons and holes [20]. The efficiency of the process is contingent on several factors, including the level of light irradiation, the catalyst loading, the initial concentration of the pollutant and photocatalyst, and the physicochemical characteristics of the water, such as its pH level or the presence of inorganic salts [21,22].

So far, there has been a paucity of studies investigating the applicability of photocatalytic degradation of MPs. In 2019, Ariza-Tarazona et al. [23] reported a mass loss of 3 % when 700–1000 μm HDPE MPs were treated during 20 h with visible light irradiation in the presence of a $\text{N}-\text{TiO}_2$ semiconductor. Moreover, Ariza-Tarazona et al. [24] observed that working with the same material with sizes around 725 μm a 70 % of mass loss was obtained with a $\text{C},\text{N}-\text{TiO}_2$ catalyst when the media was acidified to pH 3 and the temperature was cooled to 0 °C. Vital-Grappin et al. [25] observed a 29 % carbonyl index rise, ascribed to a chemical modification of the HDPE MPs, when using $\text{C},\text{N}-\text{TiO}_2$ photocatalyst. Easton et al. [26] employed different doses and intensities of UV light with H_2O_2 to degrade PET microfibers and obtained a mass loss of 23.1 % after 9 h. Uoginté et al. [27] degraded 300–1000 μm PE MPs employing different catalysts based on Cu_2O , MnO_2 and TiO_2 semiconductors achieving a 48 %, 40 % and 51 % of mass loss after 8 h, respectively. These research articles represent a first approach to the photodegradation of MPs without achieving noteworthy degradation results. Therefore, exploring the feasibility and trying to shed light on the photodegradation mechanisms of MPs is an untapped output which may help to degrade these pollutants from water.

So far, there is scarce evidence in the literature regarding the effective photocatalytic degradation of MPs. The novelty of this research lies in evaluating the photodegradation performance and providing new evidence of the photocatalytic degradation of MPs. PE MPs were selected as a model target pollutant, using commercial TiO_2 P25 under UV light irradiation, while analyzing different operational variables. Furthermore, a thorough investigation into a photocatalytic treatment is undertaken via a multiple cycles procedure with the aim of enhancing the degradation of MPs. Moreover, an exhaustive evaluation of the influence of reactive oxygen species on the photocatalytic degradation is carried out and a polymeric chain breakage mechanism is proposed. Finally, the presence of intermediates such as short-chain compounds due to the polymeric chain cleavage confirms the proposed mechanism. These evidences as well as changes in dissolved organic carbon concentration and CO_2 formation are presented. Summing up, the results

reported in this work contribute to the comprehension of new insights of the photocatalytic oxidation of MPs in the degradation of these contaminants from polluted water sources. This work could contribute to the implementation of Directive (EU) 2024/3019 that promotes a quaternary treatment as a required process to remove a wide range of micropollutants—including microplastics—from urban wastewater.

2. Materials and methods

2.1. Materials

Titanium Dioxide (TiO_2) Aerioxide® P25 was supplied by Evonik. P-benzoquinone (BQ), total organic carbon (TOC) standard ($\text{C}_8\text{H}_5\text{O}_4\text{K}$) and acetic acid were purchased from Sigma-Aldrich, and tert-butyl alcohol ($t\text{-BuOH}$) 99.5 % by Acros Organics. Formic acid (FA) 85 % from Panreac was used. Succinic acid, fumaric acid, maleic acid, oxalic acid and absorbent pads (Millipore) were purchased by Merck. All chemicals were used as received without further purification and solutions are prepared with ultrapure water (18 MΩ·cm, Millipore). Fluorescent green PE microspheres with a size of $231 \pm 19 \mu\text{m}$ were provided by Cospheric.

2.2. Experimental procedure

To achieve evidences that could confirm the photocatalytic degradation mechanism, PE microspheres were selected as model MPs. It is remarkable that PE was selected since they have density values lower than water [28], implying an additional issue [29] compared with well-dispersed MPs. As a remarkable novelty to solve this problem, an experimental set-up was designed to enhance the contact between the photocatalyst and the PE MPs. Petri dishes were selected as the reaction vessel to have as much surface exposed to light as possible. Furthermore, UV light lamps were placed just 2 cm up from the reaction vessel to ensure a proper irradiation on the photocatalyst and the MPs. The experimental set-up is shown in Fig. 1.

For the photocatalytic experiments, a determined concentration of TiO_2 was dispersed during 5 min using an ultrasonic bath (Elmasonic Select 30 FischerBrand, Fischer Scientific), with a frequency of 37 kHz. Then, the photocatalyst was placed in the Petri dishes and mixed by continuous stirring with 10 mg of MPs to ensure an initial concentration of MPs of 0.5 g L^{-1} . After reaching the specified contact time, MPs were collected from the suspension using absorbent pads (Millipore) and washed with ultrapure water to remove the photocatalyst that remains on the surface of the MPs. Finally, MPs were dried in an oven at 80 °C overnight. Experiments were performed under UV-A (365 nm) and UV-C (278 nm) LED lamps and the average irradiance that reaches the reaction system were $128 \pm 21 \text{ W m}^{-2}$ and $120 \pm 26 \text{ mW m}^{-2}$, respectively, measured using a photo-radiometer Delta Ohm HD2102. Moreover, experiments under simulated solar light were performed within a solar box (CO.FO.ME.GRA) equipped with a Xenon lamp positioned at a distance of 15 cm on the reaction vessel, with an irradiance of 203 W m^{-2} .

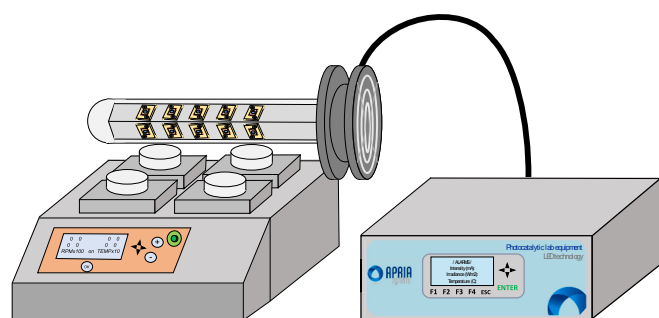


Fig. 1. Photocatalytic experimental set-up from APRI SYSTEMS, S. L. for MPs degradation.

and 57 W m^{-2} in the UV-A and visible range.

2.3. Analytical methods

Several techniques were performed to evaluate the degradation of PE MPs. The MPs mass loss was analyzed with a lab balance (OHAUS Pioneer Precision) and the reduction of the particle size was measured with a stereo microscope (Nikon SMZ18), equipped with a green fluorescence filter (light wavelength $\sim 550 \text{ nm}$) and a Jenoptik ProgRes C5 camera. Images were taken and studied using the ProgRes® CapturePro software (CapturePro V2.10.0.0), which enables to quantify the diameter of the PE microspheres. Particle size distributions were performed by analyzing samples of 20 microspheres. Morphological characterization was obtained by scanning electron microscopy (SEM) using Carl Zeiss, model EVO MA15 microscope. The images were analyzed by ImageJ software, version 1.54d. Furthermore, the MPs surface composition was evaluated with a Fourier-transform infrared (FT-IR) spectroscopy, using a Perkin Elmer Spectrum 65 spectrometer; the measurement was carried out in reflectance mode between 400 and 4000 cm^{-1} , with a resolution of 4 cm^{-1} , 150 scans and a step speed of 2 mm s^{-1} . From the FT-IR spectra, the carbonyl index (CI) was calculated by Eq. (1) [30].

$$CI (-) = \frac{\text{Absorbance}_{\text{Carbonyl band } (1720 \text{ cm}^{-1})}}{\text{Absorbance}_{\text{Reference band } (1380 \text{ cm}^{-1})}} \quad (1)$$

The generation of hydroxyl radicals in photocatalytic experiments was evaluated according to the method described in literature [31]. Briefly, this method proposes the reaction between hydroxyl radicals and dimethyl sulfoxide (DMSO) to generate formaldehyde, which then reacts with 2,4-dinitrophenylhydrazine (DNPH) to form the corresponding hydrazone (HCHO-DNPH) and was analyzed by High Performance Liquid Chromatography. The generation of hydroxyl radicals and the presence of subproducts in the water matrix were evaluated using a High-Performance Liquid Chromatography (HPLC) equipped with an Agilent Zorbax 80 Å Extend-C18 column ($5 \mu\text{m}$, $3.0 \times 150 \text{ mm}$) coupled to a diode array detector (1260 DAD-HS). To quantify the production of hydroxyl radicals, ultrapure water and methanol were the mobile phases in a ratio 40/60, a flow rate of 0.6 mL min^{-1} , and $2 \mu\text{L}$ as injection volume. In the analysis of the intermediate products, ultrapure water and acetonitrile are the mobile phases in a ratio 75/25, a flow rate of 0.2 mL min^{-1} , and $50 \mu\text{L}$ as injection volume. The quantification of the short-chain acid byproducts was determined in an ion chromatograph with autosampler, Dionex ICS5000 using Na_2CO_3 9 mM as mobile phase with an anionic column IonPac AS9-HC ($4.0 \times 50 \text{ mm}$) from Thermo Scientific and a flow rate of 1.0 mL min^{-1} . The Total Organic Carbon was used to measure the intermediates dissolved in the water in a Shimadzu TOC-V-CPH analyzer provided with autosampler.

In addition, the CO_2 production was examined using a gas chromatograph GC2010 Plus with thermal conductivity detector (TCD), a Shin Carbon ST 80/100 column and a detection limit of $7.5 \mu\text{mol}$ using argon as a carrier gas. The photocatalytic experiments were carried out in a lab-scale photo-reactor operating in batch mode, consisting of a cylindrical borosilicate glass flask with a capacity of 100 mL with two outlets to allow sample collection [32]. The photo-reactor had an illuminated surface of 290 cm^2 , and the gas volume was 30 mL . It was surrounded by four fluorescent UV-A lamps with 12.5 W m^{-2} irradiance each and 9 W of power consumption.

Finally, for the analysis of reactive oxygen species (ROS), 1.0 g L^{-1} of BQ, 46.5 g L^{-1} of t-BuOH and 4.0 g L^{-1} of FA were employed as scavengers to inhibit $\cdot\text{O}_2^-$, $\cdot\text{OH}_{\text{free}}$; and $\cdot\text{OH}_{\text{free}}$, $\cdot\text{OH}_{\text{ads}}$ and h^+ , respectively. The concentrations were set based on previous results [33].

Regarding the characterization of the commercial TiO_2 , the particles' dimensions were characterized by transmission electron microscopy (TEM) in a Jeol JEM 1011 microscope, and information about the structure of the commercial photocatalyst analyzed by X-ray diffraction

(XRD) obtained in a Bruker D8 Advance instrument fitted with a Cu tube with a wavelength of 0.15418 nm , the spectrum was collected at 2θ angles between 5 and 80° .

The Raman measurements were conducted using a confocal Raman spectrometer NRS 4100 Jasco to analyze the MPs and TiO_2 before and after the treatment. Finally, the analysis of the absorption of the photocatalyst in the UV-Vis range was performed in a UV-1800 spectrophotometer from Shimadzu.

The phytotoxicity of the samples was assessed using the Phytotestkit microbiotest supplied by MicroBio Tests Inc. These tests, which were in accordance with ISO standard 18763, enabled the evaluation of seed germination and plant growth for the specie *Lepidium sativum*. The procedure entailed the germination of seeds by adding 20 mL of the sample to the test plates, followed by a growth period of 72 h at a temperature of 25°C . Samples were used with and without MPs, to study the influence of the MPs on seed growth. MPs were removed from the liquid media with the absorbent pads. Also, measurements were made on samples with and without catalyst, evaluating whether commercial TiO_2 contributes phytotoxicity to seed growth. Samples without catalyst were previously filtered through $0.45 \mu\text{m}$ Nylon syringe filters. Comparative control tests were also carried out using 20 mL of the water matrix. The number of germinated seeds was then determined at the beginning, middle and end of the photocatalytic treatment, together with root and shoot measurements. The results were processed using the ImageJ software, version 1.54d. The seed was considered germinated if it exhibits a root or shoot length exceeding 1 mm . Based on these values, the Germination Index (GI) is calculated using the Eq. (2).

$$GI (\%) = \frac{RSG \overline{RRG}}{\overline{RSG} \overline{RRG}} \cdot 100 \quad (2)$$

where RSG is the number of germinated seeds in the sample plate, RRG is the root growth in the sample plate, \overline{RSG} is the average of germinated seeds in the control, and \overline{RRG} is the average root or shoot growth in the control plates.

3. Results and discussion

3.1. Influence of the type of irradiation

Initially, blank experiments with magnetic stirring were performed in dark conditions for 3 h . Commercial TiO_2 P25 was selected as the

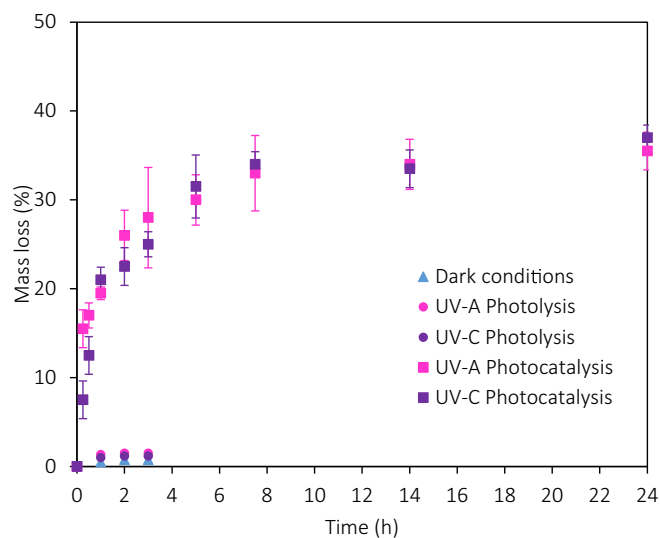


Fig. 2. PE MPs mass evolution in dark conditions, photolysis and photocatalytic experiments with 0.5 g L^{-1} of MPs and TiO_2 under different types of UV light irradiated, UV-A (365 nm) and UV-C (278 nm).

catalyst. A basic characterization is provided in the Supplementary Information (Fig. S1). As shown in Fig. 2, the results revealed that there was no significant loss of mass, since its variation was lower than 2 %. Photolysis experiments employing different UV light sources, UV-A and UV-C, and continuous stirring were performed to determine whether the MPs undergo degradation due to the exposure to UV light irradiation, or by abrasion because of the stirring process. The results showed that after 3 h under UV-A or UV-C lamps, there was no substantial MPs mass loss throughout the experiment, with an average value of 3 % and independently of the light source.

When performing photocatalytic experiments with 0.5 g L^{-1} of TiO_2 as photocatalyst, the MPs mass loss significantly increased for both types of UV light irradiated compared to dark and photolysis experiments. UV photocatalytic experiments showed a reduction in the mass of PE as exposure time increased, with mass losses of $30 \pm 2.8\%$ and $31.5 \pm 3.5\%$ after 5 h under UV-A and UV-C light, respectively. However, the rate of mass loss decreased thereafter. As observed in Fig. 2, the obtained results surpass some previously reported data. For example, Llorente-García et al. [34] reported a 4.65 % mass loss of HDPE spheres ($382 \pm 154 \mu\text{m}$) after 50 h, while Ariza-Tarazona et al. [35] reported a 16.22 % mass loss of PET microfibers after 120 h of treatment.

Comparing the photocatalytic experiments carried out under different UV lights, a similar kinetic performance is observed despite the different irradiation values in the photoreactor with $128 \pm 21 \text{ W m}^{-2}$ and $120 \pm 26 \text{ mW m}^{-2}$ for UV-A (365 nm) and UV-C (278 nm), respectively. Moreover, chemical actinometry with potassium ferrioxalate, was employed to study the quantity of photons per time ($\text{mol photons s}^{-1}$) reaching the photocatalyst. Results depicted higher irradiation of UV-A light compared to UV-C light in agreement with the higher irradiance values with an average of $3.09 \times 10^{-6} \pm 4.55 \times 10^{-7} \text{ mol photons s}^{-1}$ and $1.62 \times 10^{-8} \pm 3.17 \times 10^{-9} \text{ mol photons s}^{-1}$ for UV-A and UV-C light respectively. Nevertheless, the enhanced degradation results can be explained by an increase in the absorption of photons at 278 nm by TiO_2 . That enhanced absorption is confirmed with the UV-Vis spectra (Fig. S2). When conducting experiments under solar light, as shown in Fig. S3, lower mass loss results were obtained (18.5 %) after 5 h under simulated solar light with an irradiance of 203 W m^{-2} and 57 W m^{-2} of visible and UV-A, respectively. This reduced degradation is attributed to the lower photon absorption efficiency of this photocatalyst within this spectral range.

Moreover, the particle size distribution of the PE MPs after different times of photocatalytic treatment is shown in Fig. 3. The figure depicts that the size of initial beads (mean diameter $\approx 234 \pm 12 \mu\text{m}$) was significantly reduced after 8 h of treatment; in particular 20 % and 25 % of the particles reached sizes below 180 μm with an average diameter of $190 \pm 12 \mu\text{m}$ and $185 \pm 13 \mu\text{m}$ using UV-A and UV-C light, respectively. These results proved that the photodegradation treatment achieved a reduction in the particle diameter of the microspheres compared to the initial particles. A breakthrough of this research is that despite the reduction in the rate of mass loss, the diameters of the particles kept on decreasing throughout the experiments, thereby providing substantial evidence to support the hypothesis that MPs are undergoing a degradation process. Although in terms of mass loss UV-A and UV-C light irradiation performed similarly, the use of UV-C contributed to a greater reduction in the particle size of MPs as depicted in Fig. 3.

Fig. 4 shows the FT-IR spectra of the PE microspheres degraded after 24 h of treatment using two different UV light irradiation sources. Regarding the spectrum of initial polyethylene MPs, bands in the range of $500\text{--}800 \text{ cm}^{-1}$ were attributed to the C—C stretching vibrations, while the band located at around 1000 cm^{-1} was attributed to the coupling of the rocking of CH_2 and CH_3 . Finally, the intense bands at 1460 cm^{-1} and in the range of $2780\text{--}2970 \text{ cm}^{-1}$ were assigned to the bending vibration and stretching mode of CH_2 , respectively [36,37]. In the two samples of degraded PE MPs, titania was attached to their surface during the photocatalytic treatment, thus, all the spectra show an intense band at a wavelength around 420 cm^{-1} , corresponding to the

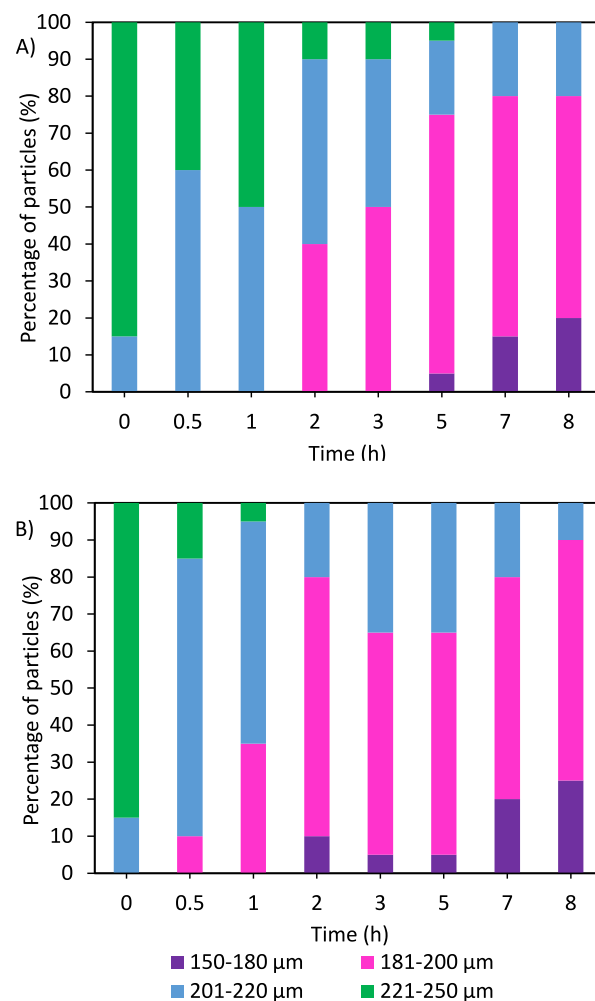


Fig. 3. PE MPs particle size distribution in experiments under different types of UV light irradiated, A) UV-A (365 nm) and B) UV-C (278 nm), using 0.5 g L^{-1} of photocatalyst and MPs.

Ti—O bond of TiO_2 [38], that remain on the MPs after the washing step. FT-IR spectra also showed the appearance of new bands for the MPs treated by photocatalysis, the bands between 3700 and 3100 cm^{-1} may be related to the presence of adsorbed water after the drying step and the formation of hydroxyl and hydroperoxyl groups displaying the onset and spread of the degradation [39]. The band of the carbonyl group at 1720 cm^{-1} [40,41], even though it was not clearly visible, is crucial to quantify the degradation of MPs. Two significant bands appeared in the degraded MPs sample at 1216 and 1152 cm^{-1} corresponding to the carboxyl functional groups (COOH) on the surface of the MPs [42]. These modifications could be attributed to the reactive oxygen species that react with the polyethylene's surface, breaking the polymeric bonds and contributing to the formation of carboxyl groups. Finally, it was observed the presence of the vinyl group at 909 cm^{-1} , indicative of the Norrish reaction of the carbonyl group under UV light exposure [43]. Similar FT-IR spectra were obtained for both UV-A and UV-C irradiation, confirming that the degradation mechanism is independent of the type of UV irradiation source employed in this work.

As the formation of carbonyl groups is a key asset to confirm the degradation of MPs, Table 1 exhibits the CI evolution. The results confirmed that it increased with time, tracking a similar trend to the mass loss, reaching enhancements of 58.5 % and 43.4 % under UV-C and UV-A light after 24 h of treatment, respectively. These results suggest a more favorable chemical transformation of PE during photocatalytic experiments under UV-C light compared to UV-A light due to the

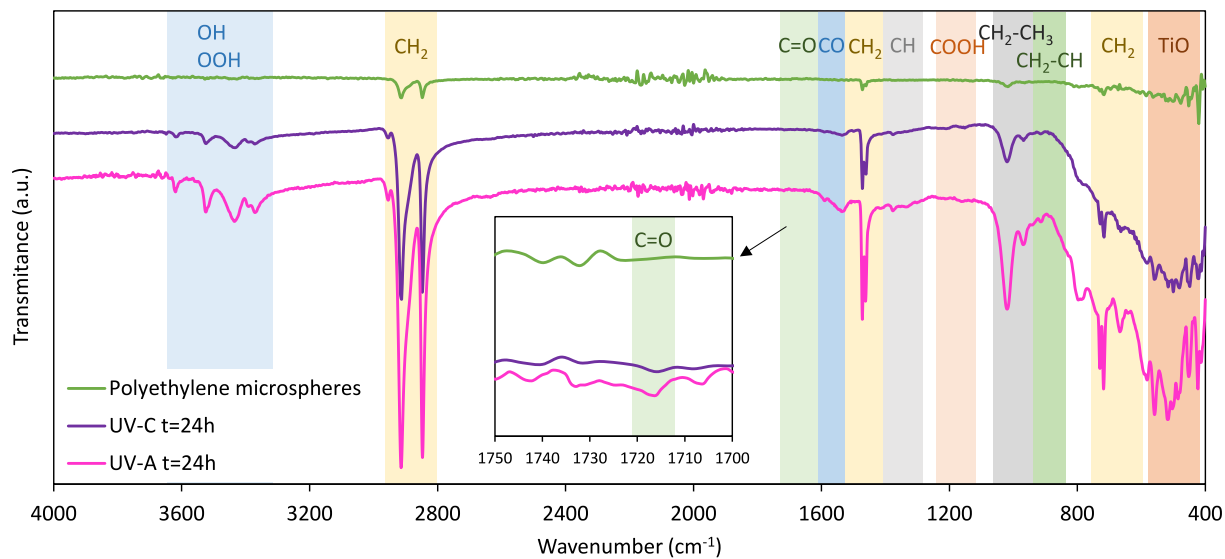


Fig. 4. FT-IR spectra in samples after 24 h of photocatalytic treatment with 0.5 g L^{-1} of photocatalyst and different types of UV light irradiation.

Table 1

Calculated carbonyl index in experiments after 24 h of photocatalytic treatment with 0.5 g L^{-1} of photocatalyst and different types of UV light irradiation sources.

Treatment type	CI (–) before treatment	CI (–) after 24 h of treatment	CI increase (%)	Mass loss (%) after 24 h of treatment
UV-A light (365 nm)	0.53	0.76	43.4	37.0 ± 1.4
UV-C light (278 nm)	0.53	0.84	58.5	35.5 ± 2.1

different number of photons received in both systems.

Comparing these CI results with literature, Vital-Grappin et al. [25] achieved 29 % CI enhancement with a 71.7 % of MPs degradation after 50 h of experiment with C,N-TiO₂ materials, and Easton et al. [26] observed a 10.6 % CI increase on PET microfibers employing UV-C/H₂O₂ technologies. Therefore, under the selected working conditions of this work, major chemical modifications than in literature have been achieved.

Additionally, the chemical modification on the surface of the microspheres is also confirmed in the Raman spectra as shown in Fig. 5. In

the spectral region from 1000 to 1700 cm⁻¹, the initial PE MP bands between 1400 and 1480 cm⁻¹ correspond to methylene bending vibrations ($\delta(\text{CH}_2)$). The crystalline phase is represented by the peak at 1419 cm⁻¹ (crystallinity band). This band is in conjunction with a crystal field splitting phenomenon, which results from an interaction between the two chains of the orthorhombic unit cell in all-trans conformation. The band at 1091 cm⁻¹ is assigned to the amorphous phase with PE chains in gauche conformation. That band has been used to determine the amount of the amorphous fraction of the material. The Raman peaks at 1064 and 1132 cm⁻¹ are attributed to the symmetric and asymmetric C=C stretching vibrations, respectively. The band with the highest intensity at 1296 cm⁻¹ is attributed to the methylene twisting vibrations ($\tau(\text{CH}_2)$), which is the main band used as internal intensity standard of polyethylene [44].

After the photocatalytic treatment several bands appear as evidence of the photocatalytic degradation of the microspheres. The bands at 1600 and 1535 cm⁻¹ are associated with the asymmetric vibrations of the conjugated C=C bonds in conjugated systems, especially when they are substituted with electronegative groups such as oxygen in this work. At 1382 cm⁻¹, there is a band corresponding to deformations of methyl (CH₃) or methylene (CH₂) groups. Finally, the band at 1170 corresponds to C—O vibrations in esters, ethers, alcohols or with C=C bonds in oxygenated chains [45]. The appearance of these bands supports another evidence into the effective photocatalytic degradation of PE MPs.

In Fig. S4, the Raman spectra of the photocatalyst confirm the evidence of the typical features of the TiO₂ anatase with the bands at 397 (B1g), 516 (A1g), 519 (B1g), and 640 cm⁻¹ (Eg). Thus, these results agree with the XRD pattern. Moreover, after 5 h of photocatalytic treatment, Raman spectra keep showing the same bands which means that under the photocatalytic degradation of MPs the catalyst structure does not change.

So, under the conditions of this work, both UV-A and UV-C were able to promote the photocatalytic degradation of PE using TiO₂ as a photocatalyst achieving similar mass loss of MPs in both cases. Nevertheless, UV-C was selected for further experiments due to the more favorable trend in the carbonyl index and particle size reduction.

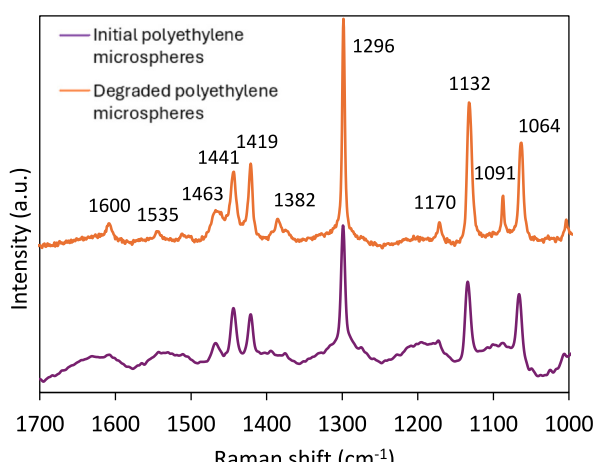


Fig. 5. Raman spectra of the PE MPs before and after 24 h of photocatalytic treatment with 0.5 g L^{-1} of photocatalyst under UV-C light irradiation.

3.2. Effect of the photocatalyst dosage

After having analyzed the feasibility of the photocatalytic degradation of PE MPs, the influence of the concentration of the photocatalyst was studied under UV-C irradiation. The initial concentration of PE MPs

in the suspension was 0.5 g L^{-1} while the concentration of the photocatalyst was varied in each experiment: 0.25 g L^{-1} , 0.5 g L^{-1} and 1 g L^{-1} . Fig. 6 shows the percentage of MPs mass loss obtained by varying the photocatalyst / MPs mass ratio. For all the experiments, it is observed that the degradation results exhibited a similar kinetic performance at the initial reaction times ($t < 2 \text{ h}$), and a significant slowdown in the mass loss kinetics is evidenced for longer operation times ($t > 5 \text{ h}$). The photocatalyst concentration has a significant impact on the photocatalytic performance; however, high concentrations cause a shielding phenomenon due to the increase in the turbidity. This phenomenon has the potential to diminish the transmittance of UV light across the reactor [46,47], while low concentrations may result in reduced generation of reactive oxygen species, thereby limiting pollutant degradation. As a result, a trade-off arises that determines the optimum catalyst concentration.

Regarding the mass loss using different photocatalyst concentrations (Fig. 6), it can be observed that the best photodegradation results were obtained for a TiO_2 concentration of 0.5 g L^{-1} , with mass loss values of $32.5 \pm 6.4 \%$, $37.0 \pm 1.4 \%$ and $29.5 \pm 3.9 \%$ for 0.25 g L^{-1} , 0.5 g L^{-1} and 1 g L^{-1} respectively, after 24 h of treatment. In addition, experimental data obtained during the first 2 h prior to the attenuation of the degradation were fitted to a pseudo-first order kinetic model given by Eq. (3).

$$\frac{dC}{dt} = -k C \quad t = 0 \rightarrow C = C_0 \quad (3)$$

where C is the MPs concentration (g L^{-1}) at time “ t ”, C_0 is the initial MPs concentration (g L^{-1}), k is the kinetic constant value (min^{-1}) and t is the experimental time (min). The values obtained for the kinetic constants are 3.5×10^{-3} , 4.1×10^{-3} and $2.8 \times 10^{-3} \text{ min}^{-1}$ for 0.25 , 0.5 and 1 g L^{-1} , respectively, with a deviation expressed as R^2 of 0.89 , 0.90 and 0.96 , respectively.

Fig. 7 displays how the particle diameters were shifted towards smaller values as the reaction time increases. It can be seen that the particle size decreases with time for all the concentrations of TiO_2 . It is observed that after 2 h using 0.5 g L^{-1} of photocatalyst, 100 % of

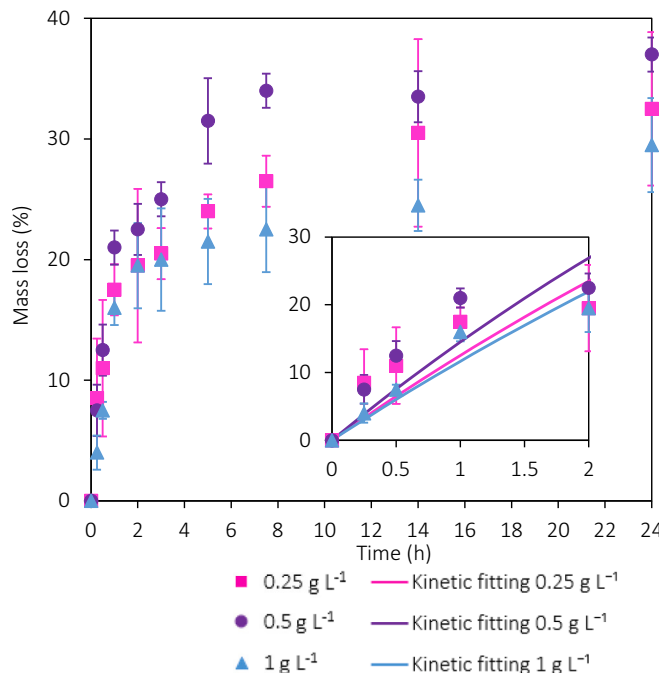


Fig. 6. PE MPs mass evolution and pseudo-first order kinetic fitting in experiments with different concentrations of photocatalyst under UV-C light irradiation and 0.5 g L^{-1} of MPs.

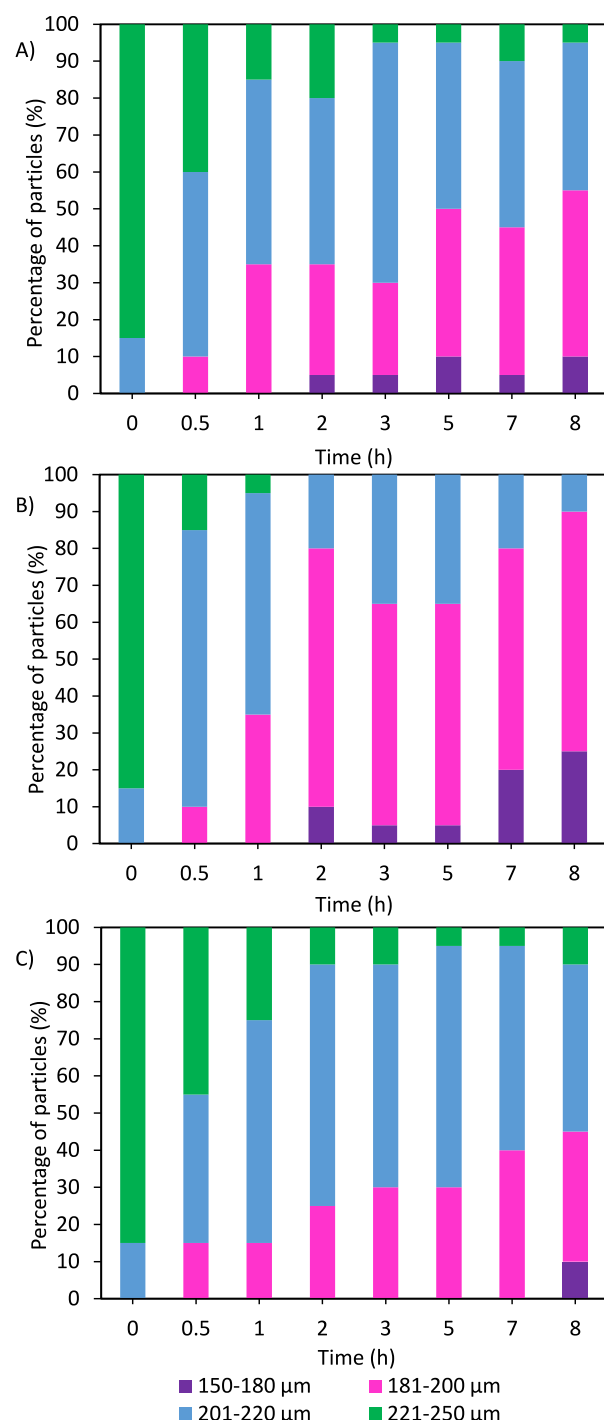


Fig. 7. PE MPs particle size distribution in experiments with A) 0.25 g L^{-1} , B) 0.5 g L^{-1} and C) 1 g L^{-1} of photocatalyst under UV-C light irradiation and 0.5 g L^{-1} of MPs.

particles with a size in the range of $221\text{--}250 \mu\text{m}$ have completely disappeared and the particles in the range of $201\text{--}220 \mu\text{m}$ led to particles with smaller sizes. Under these conditions and after 8 h of treatment, 25 % of the particles fell in the size range between 150 and $180 \mu\text{m}$; it is noteworthy that this particle size is more significant when the photocatalyst concentration is 0.5 g L^{-1} .

Fig. 8 shows the FT-IR spectra of the MPs after 8 h of UV-C light exposure employing the different concentrations of photocatalyst. It was noticed that after the photocatalytic treatment, several bands corresponding to the generation of surface carboxyl, carbonyl, vinyl and

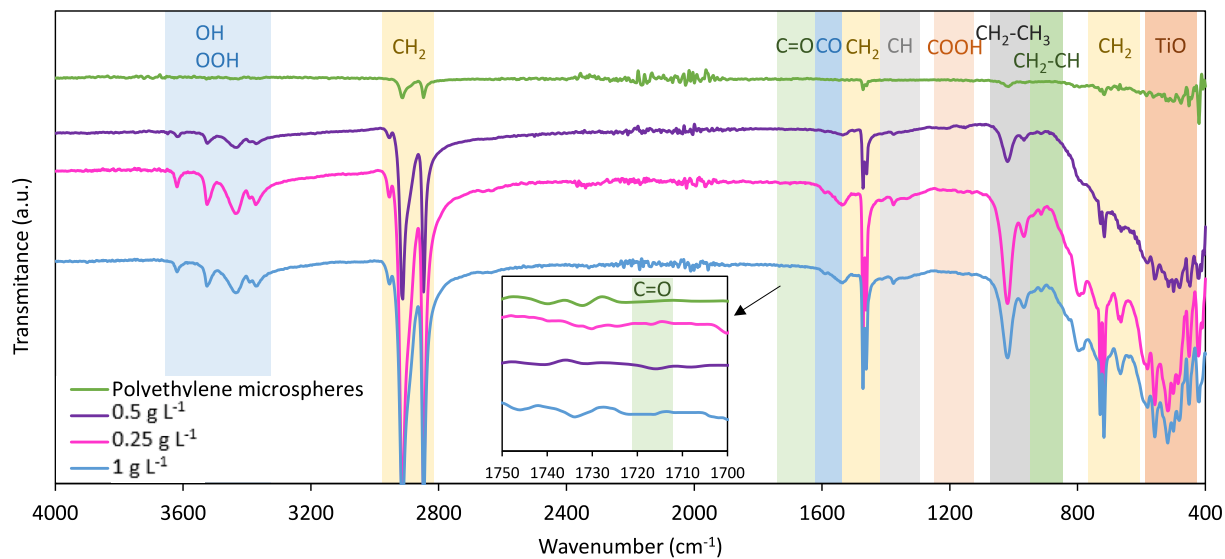


Fig. 8. FT-IR spectra in experiments with different concentrations of photocatalyst under 8 h of UV-C light irradiation and 0.5 g L^{-1} of MPs.

Table 2

Calculated carbonyl index in experiments with different concentrations of photocatalyst under 24 h of UV-C light irradiation and 0.5 g L^{-1} of MPs.

Photocatalyst concentration (g L^{-1})	CI (–) before treatment	CI (–) after 8 h of treatment	CI increase (%)	Mass loss (%) after 8 h of treatment
0.25 g L^{-1}	0.53	0.72	35.8	26.5 ± 2.1
0.5 g L^{-1}	0.53	0.84	58.5	34.0 ± 1.4
1 g L^{-1}	0.53	0.70	32.1	22.5 ± 3.5

hydroxyl groups appear, thus confirming the degradation of the PE MPs.

Moreover, the CI evaluation was carried out to compare the different FT-IR spectra (Table 2). It is noticeable that the CI underwent a considerable increase, demonstrating a significant degradation. For experiments with $0.5 \text{ g TiO}_2 \text{ L}^{-1}$, the CI value increased by 58.5 % compared to the original value (0.53), whereas concentrations of 0.25 g L^{-1} and 1 g L^{-1} led to a 37.7 % and 32.0 % increase, respectively.

Therefore, the photocatalyst / MPs 1:1 ratio led to better performance of the photocatalytic degradation of MPs, achieving 37 % mass loss after 8 h, a particle size distribution with smaller dimensions and a considerable CI rise, highlighting that a photocatalyst / MPs ratio 1:1 is more favorable to optimize the photodegradation of PE MPs. In spite of the promising results, the operation conditions need to be optimized to avoid the slowing down of the degradation rate, which limits the efficacy of the degradation process.

3.3. Photocatalytic cycles

To evaluate if it is possible to further increase the degradation of the MPs, a procedure consisting of several photocatalytic stages with an intermediate washing step and addition of fresh photocatalyst, was performed. Briefly, photocatalytic experiments were performed under 2 h of UV-C irradiation. Subsequently, MPs are filtered and dried to be characterized. Then, the resulting MPs are resuspended in a 0.5 g L^{-1} fresh TiO_2 suspension.

Fig. 9 depicts the comparison between the performance of one experiment of 10 h and the results obtained after 5 cycles of 2 h each working under the same conditions and with the original MPs. Results showed that the operation in cycles led to an enhancement on the MPs degradation yield. This modification of the photodegradation procedure

confirmed that, upon the removal of the photocatalyst from the MPs' surface and the subsequent replacement of the photocatalyst with a fresh one, the mass loss continued to increase. The outcomes of the photocatalytic stage procedure showed an enhancement from 33.5 % of mass loss in one experiment of 10 h to 54 % working during 5 cycles of 2 h each.

Results demonstrated that the first cycle exhibited a 20 % mass loss after 2 h of treatment approaching a pseudo-first order kinetic fitting (Eq. (3)) with a kinetic constant value of $3.4 \times 10^{-3} \text{ min}^{-1}$. Nevertheless, following a thorough examination of the cycles revealed that, after the washing and drying steps and the addition of fresh photocatalyst, the photodegradation kinetics declined, yielding an average kinetic constant of $2.1 \times 10^{-3} \pm 2.6 \times 10^{-4} \text{ min}^{-1}$ in the following cycles.

Replenishment of fresh catalyst helped to increase the mass loss within the photocatalytic cycles although with lower yield than compared to the first cycle probably due to resistance of the smaller particles and to the possible physical and chemical changes in the particles surface within the oxidation treatment.

Fig. 10 displays SEM images of the microspheres before and after 10 h of 5-cycles and 1-cycle experiments. Fig. 10A confirms the spherical morphology of the commercial PE MPs with a smooth surface. As shown in Fig. 10B, after 1 cycle of 10 h, the surface is modified as a consequence of the reaction with oxidant species increasing the roughness of the surface. The appearance of surface roughness after the photocatalytic treatment has also been reported in the literature [48]. Moreover, under 5 cycles of treatment, each MPs exhibited a noteworthy photocatalytic degradation, and an increased surface modification of the MPs was detected compared to 1-cycle experiments. Particle size distribution of the MPs is also evaluated for both sets of experiments in Fig. 10D–F. Initial microspheres present a mean measured diameter of $234 \pm 12 \mu\text{m}$ with spherical shape which is consistent with the characteristics reported by the supplier. After 10 h experiment, the particle size was reduced to a mean size of $191 \pm 12 \mu\text{m}$ and particles with the initial size were not detected, thus demonstrating a complete surface modification of the MPs. Additionally, in the 2 h cycles particles smaller than $170 \mu\text{m}$ with a mean size of $179 \pm 10 \mu\text{m}$ were detected underlying a remarkable photocatalytic degradation of the MPs.

The CI of the PE MPs was determined and compared for the initial microspheres and particles recovered after different photocatalytic cycles. Results showed an increase in the CI after the photocatalytic treatment compared to untreated microspheres. Nevertheless, the CI

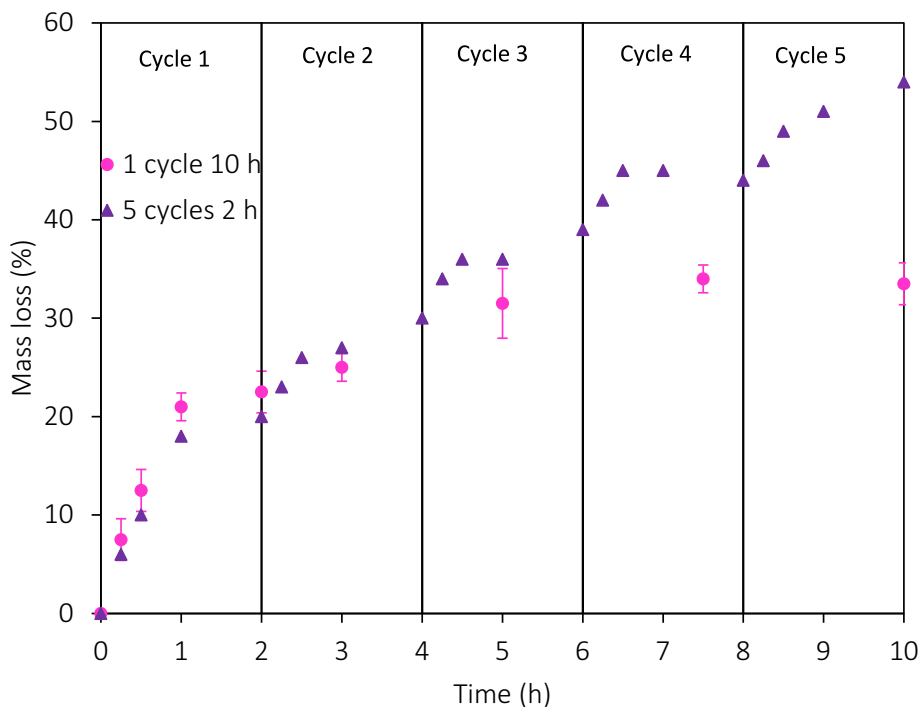


Fig. 9. MPs mass loss evolution in different cycles compared to 1 cycle experiment. Initially 0.5 g L^{-1} of PE MPs and 0.5 g L^{-1} of catalyst under UV-C irradiation.

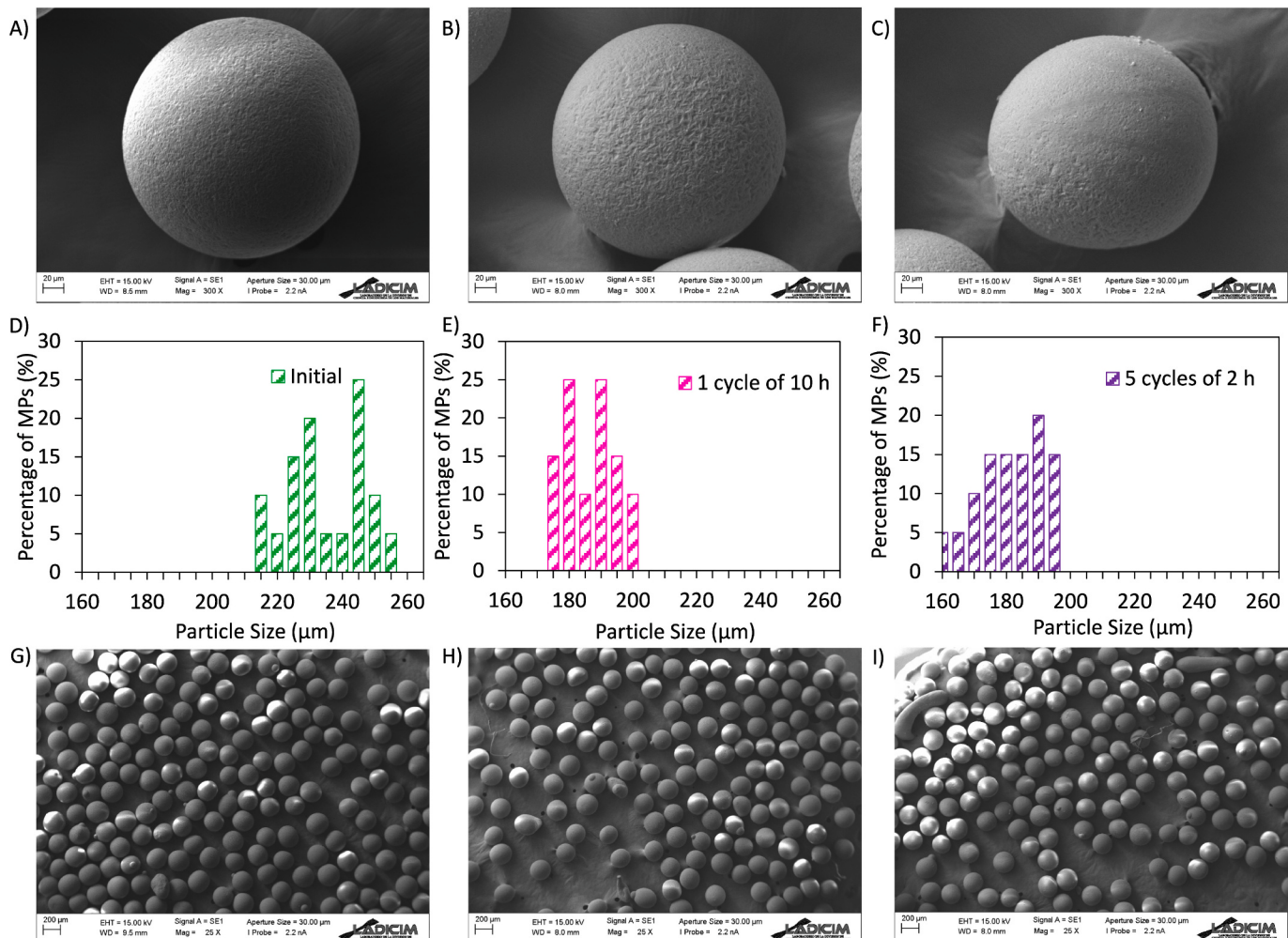


Fig. 10. SEM images and particle size distribution of A), D) and G) commercial polyethylene microspheres, B), E) and H) microspheres after 1 cycle of 10 h of UV-C irradiation and C), F) and I) microspheres after 5 cycles of 2 h of UV-C irradiation.

values did not differ from the first cycle (35.8 % increase) to the subsequent runs (26.4 ± 1.6 % increase). These similar CI values can confirm that once the radicals react with the MPs, the carbonyl functional groups on the MPs surface remain similar.

In previous works, low mass loss results are generally observed, particularly considering the long treatment times. In the comparison presented in Table S1, the work reported by Ariza-Tarazona et al. [24] shows better results after 50 h of treatment with C,N-doped TiO₂. In addition, only few studies demonstrate the enhancement of photocatalytic properties of various materials with metal or non-metal doping and heterojunctions of semiconductors. In this study, with commercial TiO₂ P25 after the photocatalytic cycles, a higher mass loss is observed under a reduced treatment time, which indicates the performance of this procedure in degrading microplastics.

3.4. Insights into the photocatalytic mechanism

To study the contribution of the radical oxidant species such as •O₂⁻, •OH_{free}, •OH_{ads} and h⁺ in the photodegradation process of PE MPs employing TiO₂ under UV-C light, scavengers, which inhibit the presence of ROS in the water matrix, were added to the aqueous medium. Fig. 11 shows the mass loss evolution of MPs incorporating the different scavengers in the treated solution. It depicts lower degradation values when BQ was used as scavenger with a mass loss reduction from 34 % (without scavengers) to 10 % (with BQ) after 8 h of experiment, concluding that O₂⁻ was actively contributing to the degradation mechanism. Even though some authors have reported the low production capability of superoxide radicals by TiO₂ P25 due to their recombination [49], this study states its remarkable impact on the MPs degradation. In addition, t-BuOH can react with the holes of the semiconductor, preventing the generation of OH[•] and oxidation of pollutants. Subsequently, •OH_{free} and •OH_{ads} were not generated. Otherwise, FA only reacted with the •OH_{free} in the media. Besides, it was noteworthy that when t-BuOH or FA were used, similar degradation results were obtained with an average mass loss of 15 %. These results were attributed to the similar performance of holes and •OH_{free}, concluding that •OH_{ads} radicals play a negligible role in the MPs degradation.

According to the results of this study and in agreement with previously reported works [25,50–53], it is possible to consider that •O₂⁻ and •OH_{free} are the primary radicals involved in the degradation of MPs. The

proposed photocatalytic degradation pathway of PE MPs is shown in Fig. 12. Polyethylene chains have the capacity to interact with hydroxyl and peroxide radicals generated by the photoexcitation of TiO₂. This interaction serves as the initiating factor for the chain degradation process. Subsequently, the propagation occurs between (-CH₂-) to form (-CH₂-HCOO[•]-CH₂-) in the presence of O₂. Then, a hydrogen atom is released from the polymeric chain resulting in the formation of hydroperoxide groups in the chain (-CH₂-HCOOH-CH₂-). This process leads to the scission of the chain into two macroradicals (-CH₂-HCO[•]-CH₂-) and HO[•] by chain scission due to the weakness of the O—O bond. The free radicals generated by the chain scission of the bond between the carbonyl group and the α-C atom (α-scission), results in the formation of CO (Norrish Type I). Intramolecular processes, such as the withdrawal of hydrogen from the γ carbon (Norrish Type II), subsequently leads to the decomposition of the polymeric chain into an unsaturated polymer chain end, resulting in the formation of carbonyl and vinyl groups (C=C). Consequently, PE degradation proceeds via Norrish Type I and II reactions (aldehyde and ketone groups). As a result, short-chain end products are produced by the degradation of the polymeric chain breakage, leading eventually to the mineralization of these compounds. In agreement with the formation of these short chain compounds, some studies have identified that the increase in the carboxylic groups can indicate the formation of short-chain acids such as acetic acid [54] and oxalic, carbonic and formic acids [55] as possible end products.

To confirm the proposed mechanisms, the concentration of •OH radicals was determined (Fig. S5). In that figure, it is observed that the generation of hydroxyl radicals in the samples during the process leads to conclude that HO[•] are continuously generated at an average kinetic rate of 3.9×10^{-3} mM min⁻¹. This significant production of hydroxyl radicals with a constant rate supported the effectiveness of the photocatalytic method in the production of ROS, a noteworthy factor for the success of the MPs photodegradation process. Moreover, the attenuation in the mass loss after 2 h cannot be directly correlated with the reduction in presence of oxidant compounds, as the deactivation of the catalyst is not observed.

Additionally, different analyses were performed to examine the presence of byproducts. Fig. 13A shows the evolution with time of the dissolved organic carbon (DOC) in the photocatalytic experiments. Results show an increase of the DOC as a consequence of the presence of organic compounds in solution due to the polymeric chain breakage. This is further confirmed with the presence of possible intermediate products by high-performance liquid chromatography (HPLC) and ion chromatography (IC). HPLC could reveal the presence of two compounds (Fig. 13B) that could not be fully identified. Further details can be found in the supplementary information.

Ion chromatography results confirmed the presence of acetic acid and formic acid, Fig. 13C. The formation of these byproducts is in agreement with the DOC analyses in which their concentration is reduced after 8 h of treatment as a consequence of the degradation and mineralization of the intermediates. Comparing these organic compounds, all of them possess a similar structure with carboxyl groups that resulted after the reaction of the polymeric chain with the reactive oxygen species. Moreover, the formation of CO₂ was analyzed by gas chromatography (Fig. S6) for experiments carried out under a controlled presence of O₂. Even though the photodegradation treatment stabilizes after a certain time, results point to the partial mineralization of the MPs with a continuous CO₂ production of 17.51 μmol after 24 h.

3.5. Analysis of different water matrices

With the objective of transferring the results of this work to more realistic conditions, an analysis of the impact of different water matrices

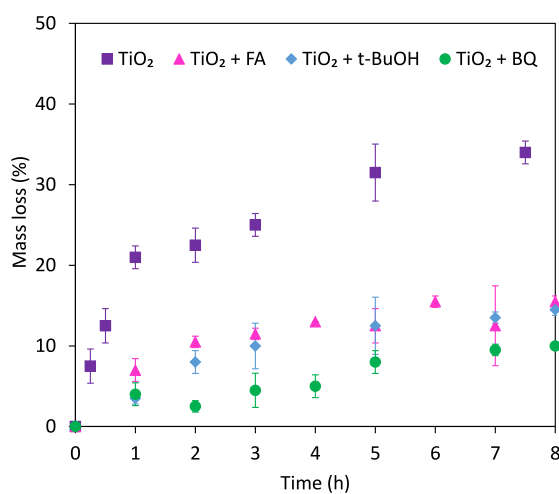


Fig. 11. MPs mass loss evolution in experiments with different scavengers with 0.5 g L⁻¹ of PE MPs and 0.5 g L⁻¹ of catalyst under UV-C irradiation.

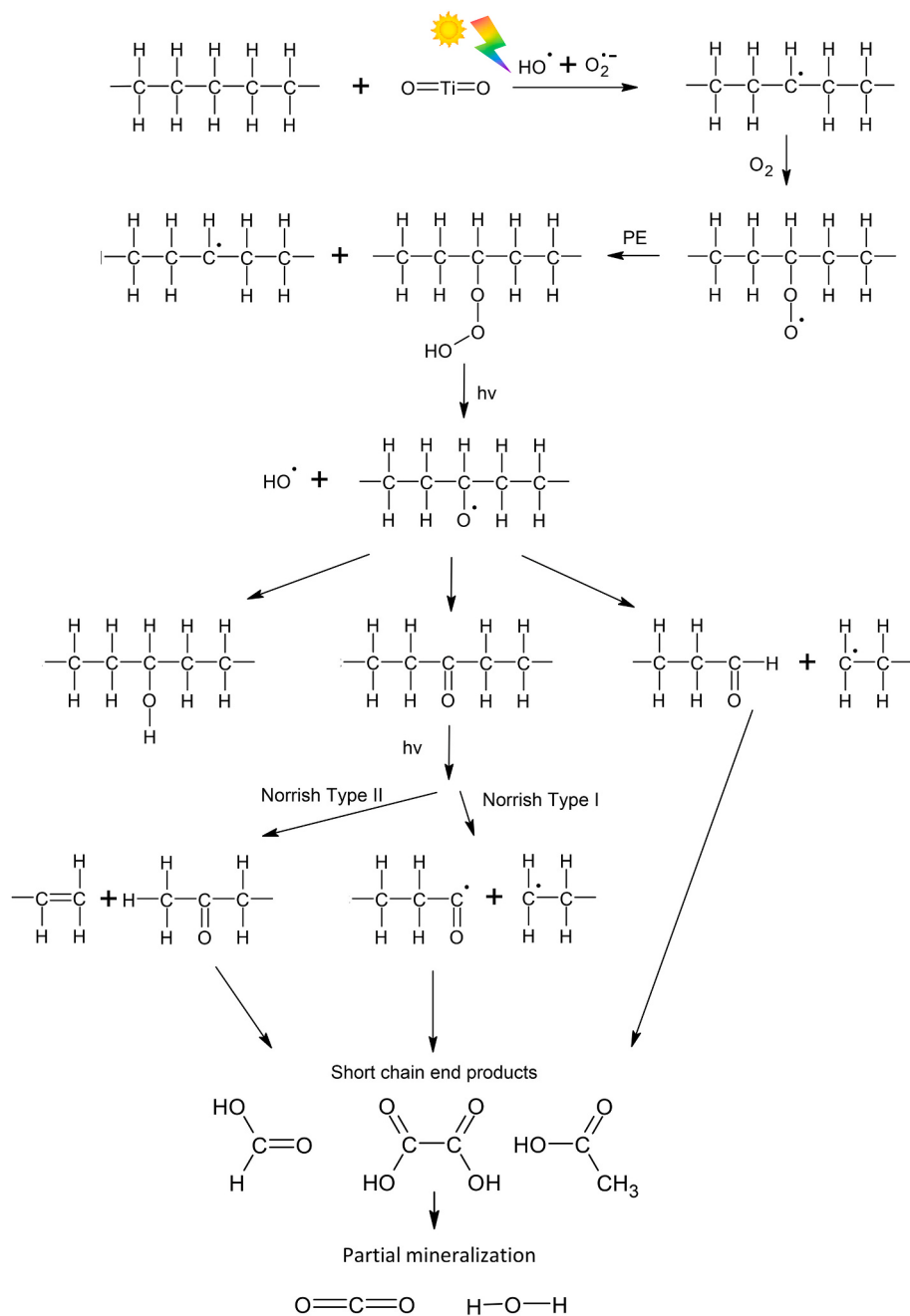


Fig. 12. Proposed mechanism for PE MPs photocatalytic degradation with commercial TiO_2 P25.

on the photocatalytic degradation of PE MPs was carried out. Ultrapure water, tap water and WWTP secondary effluent were used and their characterization is already reported [15].

The mass loss results after 5 h of UV-C photocatalytic treatment are shown in Fig. 14. When there was an increase in the ions present in the water matrix, the mass loss values were reduced, lowering to a value of $31.5 \pm 3.5\%$, $27.0 \pm 1.4\%$, $17.0 \pm 4.2\%$ and $19.0 \pm 1.4\%$ for ultrapure water, tap water, seawater and WWTP effluent, respectively. The reduction in the percentages was attributed to the possible competition of other ions with the reactive oxygen species. Nevertheless, MPs still underwent photocatalytic degradation despite the presence of salts and suspended solids using seawater and WWTP secondary effluent, respectively.

An assessment of the phytotoxicity is essential in water remediation processes, as the reaction intermediates and final products may become more hazardous than the initial contaminants [56,57]. Thereby, phytotoxicity tests were performed using the specie *Lepidium sativum*. The literature typically recognizes as the absence of phytotoxic substances if $\text{GI} \geq 80\%$ whereas $\text{GI} \leq 50\%$ is regarded as highly toxic and not suitable for water reuse in agricultural purposes [58].

Fig. 15 collects a comprehensive analysis of the GI of the roots (Fig. 15A) and shoots (Fig. 15B) of the seeds during photocatalytic experiments of 5 h. This analysis also includes the GI of the control samples, which consisted of 20 mL of the water matrix in accordance with the technical data sheet. Results showed that after the photocatalytic treatment, there was no change in the phytotoxicity of any of the water

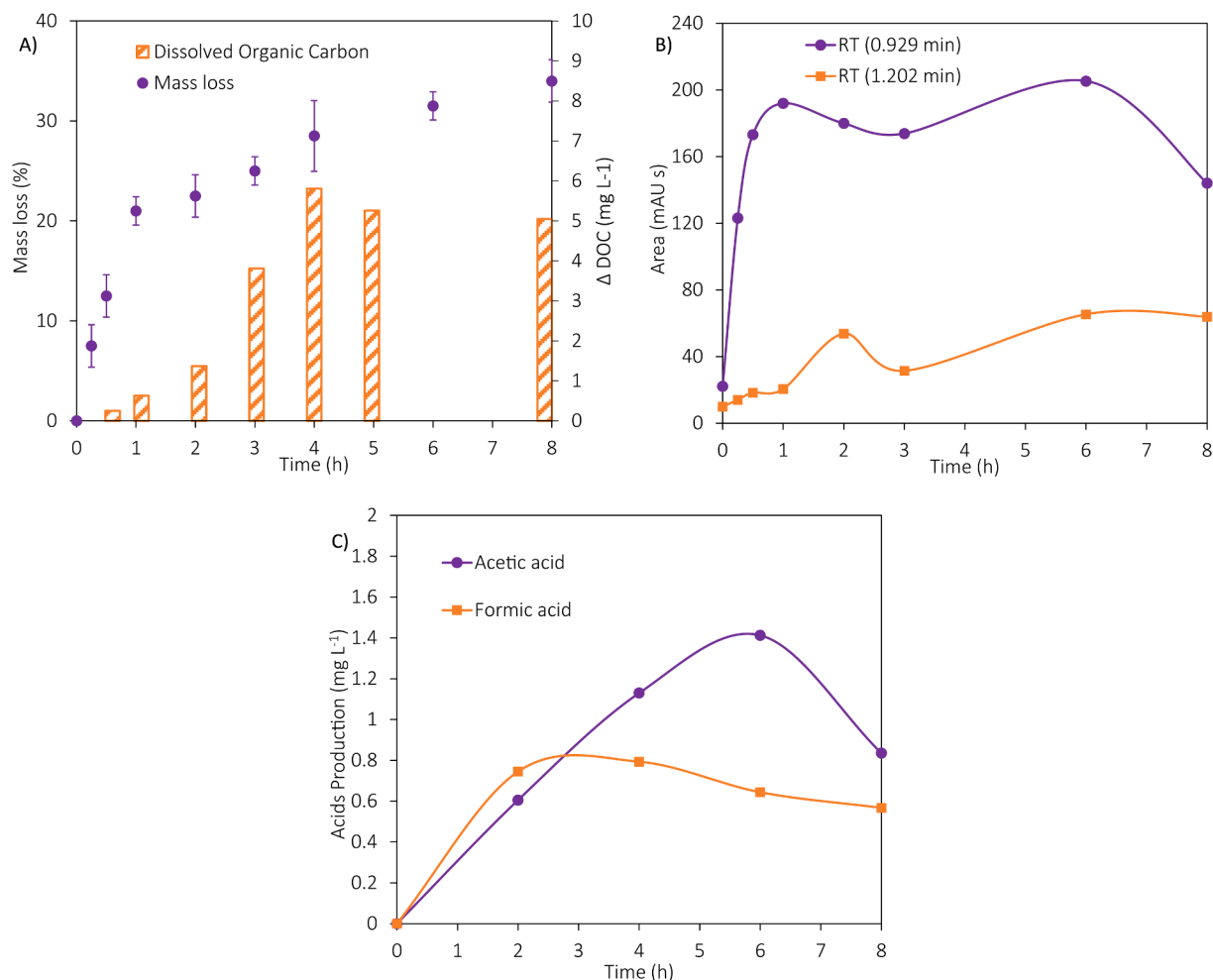


Fig. 13. A) Change over time of the MPs mass loss and dissolved organic carbon and B) and C) determined oxidation byproducts in High-Performance Liquid Chromatography (B) and Ion Chromatography (C), in experiments with 0.5 g L⁻¹ of PE MPs and 0.5 g L⁻¹ of catalyst under UV-C irradiation.

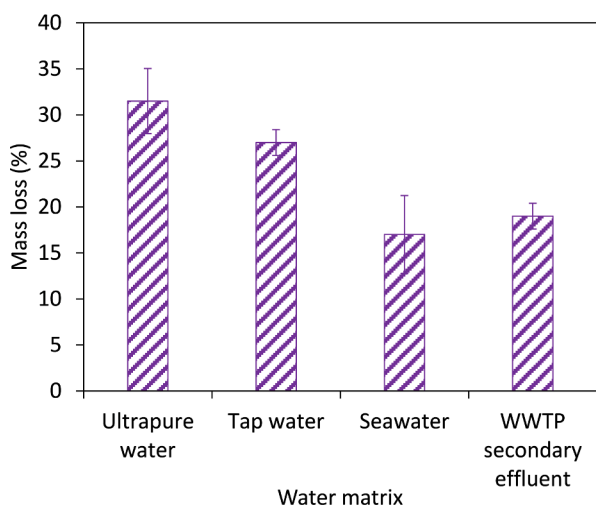


Fig. 14. PE MPs mass loss values using different water matrices after 5 h of UV photocatalytic treatment using 0.5 g L⁻¹ of photocatalyst and MPs.

matrices, with GI values $\approx 100\%$, which means that the intermediates generated during the treatment were not harmful for agricultural purposes.

To determine whether the observed differences in root and shoots length were statistically significant, a Student's *t*-test for the different samples was applied. Statistical analysis was conducted at a 95 % confidence level. A *p*-value <0.05 was considered statistically significant between the treated and control samples, suggesting a phytotoxic effect attributable to the sample. Samples with a significant error are designated with an asterisk in Fig. 15. The statistical analysis shows that the roots exhibited a similar growth compared to the control experiments of the different water bodies. In addition, both the presence of TiO₂ P25 and PE MPs did not lead to any toxicological effect. Nevertheless, when performing the study of the shoots, a notable reduction in their growth was observed in the samples within MPs. When using ultrapure water and tap water an index of potential toxicity was also observed in the first hours of treatment. However, after 5 h of treatment, the samples did not present any toxicological effect to the roots nor the shoots, highlighting the potential use of these water bodies as irrigation water.

4. Conclusions

This work aims to provide insights into the photocatalytic degradation of MPs, with particular focus on the impact of operational variables. Working with 0.5 g L⁻¹ of polyethylene MPs as a model target pollutant and commercial TiO₂ P25 as catalyst under UV light irradiation, the optimum MPs/TiO₂ mass ratio was determined as 1:1 and achieved 34.0 \pm 1.4 % of PE mass loss after 8 h of UV-C irradiation, with reduction of

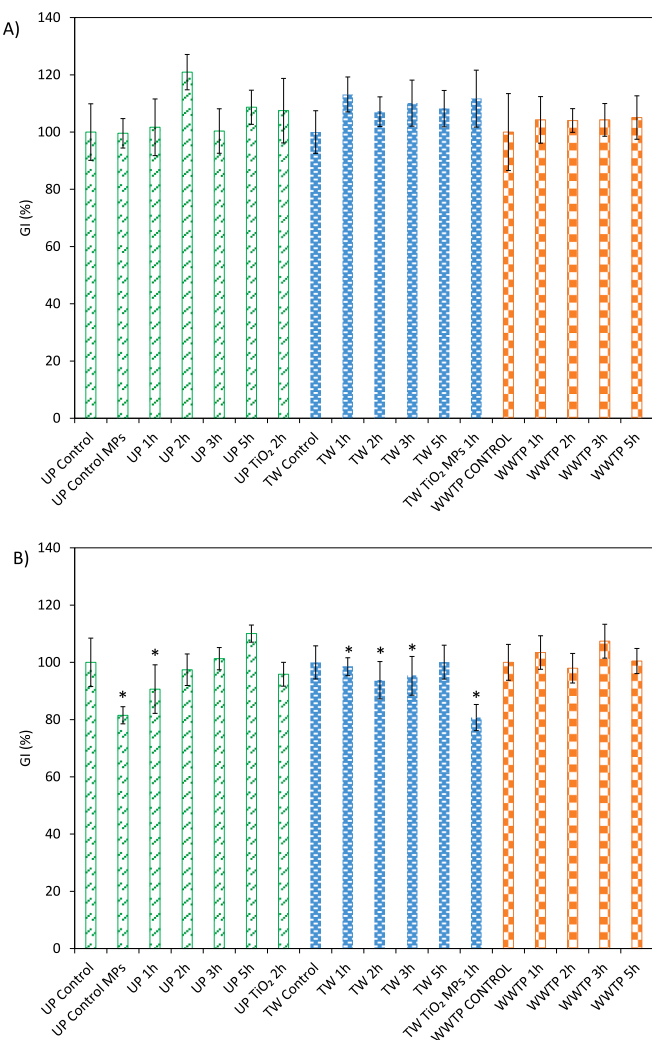


Fig. 15. Germination index obtained with *Lepidium sativum* seeds for A) roots, and B) shoots throughout the photocatalytic experiments using different water matrices.

the particle size from diameters of $234 \pm 12 \mu\text{m}$ to values smaller than $200 \mu\text{m}$ for more than 65 % of the particles. In addition to the reduction in the mass and size of the initial MPs, the formation of carbonyl, carboxyl, hydroxyl and hydroperoxyl bands in the FT-IR spectra and a 57.5 % CI rise confirmed that the particles are undergoing a degradation process with chemical changes in their structure.

Nevertheless, after 5 h of treatment, the photocatalytic degradation rates exhibited a decline. To solve that issue, a procedure consisting of several photocatalytic stages with an intermediate washing step and addition of fresh photocatalyst, was performed. The mass loss percentage was found to be 54 % after five cycles of 2 h, in comparison to 33.5 % after a single ten-hour experiment. Furthermore, following five cycles of 2 h, MPs demonstrated a substantial photodegradation, characterized by a significant reduction in particle size. Specifically, 10 % of the particles exhibited a size below $170 \mu\text{m}$, with a mean size of $179 \pm 10 \mu\text{m}$, compared to the $191 \pm 12 \mu\text{m}$ recorded after a single ten-hour experiment. Moreover, the quantification of OH^\bullet radicals revealed that their generation rate remained constant for a period exceeding 7 h of experiment. Therefore, the slowdown in the reaction rate could not be attributed to the lack of oxidant species but to physical and chemical changes on the particles' surface. Additional experiments should be carried out to confirm this hypothesis.

Finally, the contribution of different reactive oxygen species and a photodegradation mechanism are proposed. $\cdot\text{O}_2^-$ and $\cdot\text{OH}$ were found to

be actively contributing to the degradation pathway. In addition, to confirm the proposed mechanism, a survey for degradation products was conducted. Dissolved organic carbon of the water increased 5.05 mg L^{-1} after 8 h of treatment and different intermediate products and short-chain acids such as acetic and formic acid were identified in the water, as a result of the degradation of MPs. Moreover, an analysis of the CO_2 yield revealed a linear production rate, thereby emphasizing the partial mineralization of the MPs. Moreover, an analysis of the effective photocatalytic degradation in different water matrices and their toxicity was conducted, concluding that after this treatment, the treated water can be employed in irrigation applications. Overall, the results reported in this work provide evidences that contribute to the knowledge of MPs photocatalytic degradation in polluted water sources.

CRediT authorship contribution statement

Daniel Aragón: Writing – review & editing, Writing – original draft, Validation, Methodology, Investigation, Formal analysis, Conceptualization. **Carmen Barquín:** Data curation, Investigation, Writing – review & editing. **Eugenio Bringas:** Writing – review & editing, Validation, Supervision, Project administration, Methodology, Funding acquisition, Conceptualization. **Inmaculada Ortiz:** Writing – review & editing, Validation, Supervision, Conceptualization. **Maria J. Rivero:** Writing – review & editing, Validation, Supervision, Resources, Project administration, Methodology, Funding acquisition, Conceptualization.

Declaration of competing interest

The authors declare that they have no known competing financial interests or personal relationships that could have appeared to influence the work reported in this paper.

Acknowledgements

These results are part of the R&D project PID2021-122563OB-I00 funded by MICIU/AEI/10.13039/501100011033 and by “ERDF/EU”. Daniel Aragón is grateful for the grant PRE2022-104908 funded by MICIU/AEI/10.13039/501100011033 and by “ESF+”. The authors acknowledge the SERMET of the Universidad de Cantabria for TEM measurements.

Appendix A. Supplementary data

Supplementary data to this article can be found online at <https://doi.org/10.1016/j.cej.2025.166672>.

Data availability

Data will be made available on request.

References

- [1] T.A. Kurniawan, A. Haider, H.M. Ahmad, A. Mohyuddin, H.M. Umer Aslam, S. Nadeem, M. Javed, M.H.D. Othman, H.H. Goh, K.W. Chew, Source, occurrence, distribution, fate, and implications of microplastic pollutants in freshwater environment: a critical review and way forward, Chemosphere 325 (2023) 138367, <https://doi.org/10.1016/j.chemosphere.2023.138367>.
- [2] N. Parashar, S. Hait, Recent advances on microplastics pollution and removal from wastewater systems: a critical review, J. Environ. Manage. 340 (2023) 118014, <https://doi.org/10.1016/j.jenvman.2023.118014>.
- [3] C. Xiao, M. Lang, R. Wu, Z. Zhang, X. Guo, A review of the distribution, characteristics and environmental fate of microplastics in different environments of China, Rev. Environ. Contam. Toxicol. 261 (2023) 3, <https://doi.org/10.1007/s44169-023-00026-0>.
- [4] S. Sharma, S. Basu, N.P. Shetti, M.N. Nadagouda, T.M. Aminabhavi, Microplastics in the environment: occurrence, perils, and eradication, Chem. Eng. J. 408 (2021) 127317, <https://doi.org/10.1016/j.cej.2020.127317>.
- [5] A.S. Ahmed, M.M. Billah, M.M. Ali, M.K.A. Bhuiyan, L. Guo, M. Mohinuzzaman, M.B. Hossain, M.S. Rahman, M.S. Islam, M. Yan, W. Cai, Microplastics in aquatic environments: a comprehensive review of toxicity, removal, and remediation

- strategies, *Sci. Total Environ.* 876 (2023) 162414, <https://doi.org/10.1016/j.scitotenv.2023.162414>.
- [6] F. Murphy, C. Ewins, F. Carbonnier, B. Quinn, Wastewater treatment works (WwTW) as a source of microplastics in the aquatic environment, *Environ. Sci. Technol.* 50 (2016) 5800–5808, <https://doi.org/10.1021/acs.est.5b05416>.
- [7] M.B. Ahmed, M.S. Rahman, J. Alom, M.S. Hasan, M.A.H. Johir, M.I.H. Mondal, D. Y. Lee, J. Park, J.L. Zhou, M.H. Yoon, Microplastic particles in the aquatic environment: a systematic review, *Sci. Total Environ.* 775 (2021) 145793, <https://doi.org/10.1016/j.scitotenv.2021.145793>.
- [8] European Union, Directive (EU) 2019/904 of the European Parliament and of the Council of 5 June 2019 on the Reduction of the Impact of Certain Plastic Products on the Environment, <http://data.europa.eu/eli/dir/2019/904/oj>, 2019.
- [9] A. Zeb, W. Liu, N. Ali, R. Shi, Q. Wang, J. Wang, J. Li, C. Yin, J. Liu, M. Yu, J. Liu, Microplastic pollution in terrestrial ecosystems: global implications and sustainable solutions, *J. Hazard. Mater.* 461 (2024) 132636, <https://doi.org/10.1016/j.jhazmat.2023.132636>.
- [10] I.M. Belli, M. Cavali, L.H.P. Garbossa, D. Franco, R. Bayard, A.B. de Castilhos Junior, A review of plastic debris in the South American Atlantic Ocean coast – distribution, characteristics, policies and legal aspects, *Sci. Total Environ.* 938 (2024) 173197, <https://doi.org/10.1016/j.scitotenv.2024.173197>.
- [11] E.D. Okoffo, C. Rauert, K.V. Thomas, Mass quantification of microplastic at wastewater treatment plants by pyrolysis-gas chromatography-mass spectrometry, *Sci. Total Environ.* 856 (2023) 159251, <https://doi.org/10.1016/j.scitotenv.2022.159251>.
- [12] M. Pivokonsky, L. Cermakova, K. Novotna, P. Peer, T. Cajthaml, V. Janda, Occurrence of microplastics in raw and treated drinking water, *Sci. Total Environ.* 643 (2018) 1644–1651, <https://doi.org/10.1016/j.scitotenv.2018.08.102>.
- [13] Y. Xu, Q. Ou, M. Jiao, G. Liu, J.P. Van Der Hoek, Identification and quantification of nanoplastics in surface water and groundwater by pyrolysis gas chromatography-mass spectrometry, *Environ. Sci. Technol.* 56 (2022) 4988–4997, <https://doi.org/10.1016/acs.est.1c07377>.
- [14] N. Weithmann, J.N. Möller, M.G.J. Löder, S. Piehl, C. Laforsch, R. Freitag, Organic fertilizer as a vehicle for the entry of microplastic into the environment, *Sci. Adv.* 4 (2018) eaao8060, <https://doi.org/10.1126/sciadv.aao8060>.
- [15] D. Aragón, B. García-Merino, C. Barquín, E. Bringas, M.J. Rivero, I. Ortiz, Advanced green capture of microplastics from different water matrices by surface-modified magnetic nanoparticles, *Sep. Purif. Technol.* 354 (2024) 128813, <https://doi.org/10.1016/j.seppur.2024.128813>.
- [16] Y. Lu, M.C. Li, J. Lee, C. Liu, C. Mei, Microplastic remediation technologies in water and wastewater treatment processes: current status and future perspectives, *Sci. Total Environ.* 868 (2023) 161618, <https://doi.org/10.1016/j.scitotenv.2023.161618>.
- [17] European Union, Directive (EU) 2024/3019 of the European Parliament and of the Council of 27 November 2024 Concerning Urban Wastewater Treatment. <http://data.europa.eu/eli/dir/2024/3019/oj>, 2024.
- [18] S. Malato, P. Fernández-Ibáñez, M.I. Maldonado, J. Blanco, W. Gernjak, Decontamination and disinfection of water by solar photocatalysis: recent overview and trends, *Catal. Today* 147 (2009) 1–59, <https://doi.org/10.1016/j.cattod.2009.06.018>.
- [19] L. Rizzo, S. Malato, D. Antakyali, V.G. Beretsou, M.B. Dolić, W. Gernjak, E. Heath, I. Ivancev-Tumbas, P. Karaochia, A.R. Lado Ribeiro, G. Mascolo, C.S. McArdell, H. Schaar, A.M.T. Silva, D. Patta-Kassinios, Consolidated vs new advanced treatment methods for the removal of contaminants of emerging concern from urban wastewater, *Sci. Total Environ.* 655 (2019) 986–1008, <https://doi.org/10.1016/j.scitotenv.2018.11.265>.
- [20] K. Rizwan, M. Bilal, Developments in advanced oxidation processes for removal of microplastics from aqueous matrices, *Environ. Sci. Pollut. Res.* 29 (2022) 86933–86953, <https://doi.org/10.1007/s11356-022-23545-0>.
- [21] U. Kumar, J.Z. Hassan, R.A. Bhatti, A. Raza, G. Nazir, W. Nabgan, M. Ikram, Photocatalysis vs adsorption by metal oxide nanoparticles, *J. Mater. Sci. Technol.* 131 (2022) 122–166, <https://doi.org/10.1016/j.jmst.2022.05.020>.
- [22] N. Taoufik, W. Boumya, M. Achak, H. Chennouk, R. Dewil, N. Barka, The state of art on the prediction of efficiency and modeling of the processes of pollutants removal based on machine learning, *Sci. Total Environ.* 807 (2022) 150554, <https://doi.org/10.1016/j.scitotenv.2021.150554>.
- [23] M.C. Ariza-Tarazona, J.F. Villarreal-Chiu, V. Barbieri, C. Siligardi, E.I. Cedillo-González, New strategy for microplastic degradation: green photocatalysis using a protein-based porous N-TiO₂ semiconductor, *Ceram. Int.* 45 (2019) 9618–9624, <https://doi.org/10.1016/j.ceramint.2018.10.208>.
- [24] M.C. Ariza-Tarazona, J.F. Villarreal-Chiu, J.M. Hernández-López, J. Rivera De la Rosa, V. Barbieri, C. Siligardi, E.I. Cedillo-González, Microplastic pollution reduction by a carbon and nitrogen-doped TiO₂: effect of pH and temperature in the photocatalytic degradation process, *J. Hazard. Mater.* 395 (2020) 122632, <https://doi.org/10.1016/j.jhazmat.2020.122632>.
- [25] A.D. Vital-Grappin, M.C. Ariza-Tarazona, V.M. Luna-Hernández, J.F. Villarreal-Chiu, J.M. Hernández-López, C. Siligardi, E.I. Cedillo-González, The role of the reactive species involved in the photocatalytic degradation of hdpe microplastics using C,N-TiO₂ powders, *Polymers (Basel)* 13 (2021) 999, <https://doi.org/10.3390/polym13070999>.
- [26] T. Easton, V. Koutsos, E. Chatzisymeon, Removal of polyester fibre microplastics from wastewater using a UV/H₂O₂ oxidation process, *J. Environ. Chem. Eng.* 11 (2023) 109057, <https://doi.org/10.1016/j.jece.2022.109057>.
- [27] I. Uogintė, S. Pleskystė, M. Skapas, S. Stanionytė, G. Lujanienė, Degradation and optimization of microplastic in aqueous solutions with graphene oxide-based nanomaterials, *Int. J. Environ. Sci. Technol.* 20 (2023) 9693–9706, <https://doi.org/10.1007/s13762-022-04657-z>.
- [28] M.N. Issac, B. Kandasubramanian, Effect of microplastics in water and aquatic systems, *Environ. Sci. Pollut. Res.* 28 (2021) 19544–19562, <https://doi.org/10.1007/s11356-021-13184-2>.
- [29] G. Everaert, M. De Rijcke, B. Lonneville, C.R. Janssen, T. Backhaus, J. Mees, E. van Sebille, A.A. Koelmans, A.I. Catarino, M.B. Vandegheuchte, Risks of floating microplastic in the global ocean, *Environ. Pollut.* 267 (2020) 115499, <https://doi.org/10.1016/j.envpol.2020.115499>.
- [30] A. Sun, W.X. Wang, Photodegradation of microplastics by ZnO nanoparticles with resulting cellular and subcellular responses, *Environ. Sci. Technol.* 57 (2023) 8118–8129, <https://doi.org/10.1021/acs.est.3c01307>.
- [31] C. Tai, J.F. Peng, J.F. Liu, G. Bin Jiang, H. Zou, Determination of hydroxyl radicals in advanced oxidation processes with dimethyl sulfoxide trapping and liquid chromatography, *Anal. Chim. Acta* 527 (2004) 73–80, <https://doi.org/10.1016/j.aca.2004.08.019>.
- [32] D. Pelayo, M.J. Rivero, G. Santos, P. Gómez, I. Ortiz, Techno-economic evaluation of UV light technologies in water remediation, *Sci. Total Environ.* 868 (2023) 161376, <https://doi.org/10.1016/j.scitotenv.2022.161376>.
- [33] P. Ribao, J. Corredor, M.J. Rivero, I. Ortiz, Role of reactive oxygen species on the activity of noble metal-doped TiO₂ photocatalysts, *J. Hazard. Mater.* 372 (2019) 45–51, <https://doi.org/10.1016/j.jhazmat.2018.05.026>.
- [34] B.E. Llorente-García, J.M. Hernández-López, A.A. Zaldívar-Cadena, C. Siligardi, E. I. Cedillo-González, First insights into photocatalytic degradation of HDPE and LDPE microplastics by a mesoporous N-TiO₂ coating: effect of size and shape of microplastics, *Coatings* 10 (2020) 658, <https://doi.org/10.3390/coatings10070658>.
- [35] M.C. Ariza-Tarazona, C. Siligardi, H.A. Carreón-López, J.E. Valdés-Cerda, P. Pozzi, G. Kaushik, J.F. Villarreal-Chiu, E.I. Cedillo-González, Low environmental impact remediation of microplastics: visible-light photocatalytic degradation of PET microplastics using bio-inspired C,N-TiO₂/SiO₂ photocatalysts, *Mar. Pollut. Bull.* 193 (2023) 115206, <https://doi.org/10.1016/j.marpolbul.2023.115206>.
- [36] A. Käppler, F. Windrich, M.G.J. Löder, M. Malanin, D. Fischer, M. Labrenz, K. J. Eichhorn, B. Voit, Identification of microplastics by FTIR and Raman microscopy: a novel silicon filter substrate opens the important spectral range below 1300 cm⁻¹ for FTIR transmission measurements, *Anal. Bioanal. Chem.* 407 (2015) 6791–6801, <https://doi.org/10.1007/s00216-015-8850-8>.
- [37] M. Shen, B. Song, G. Zeng, Y. Zhang, F. Teng, C. Zhou, Surfactant changes lead adsorption behaviors and mechanisms on microplastics, *Chem. Eng. J.* 405 (2021) 126989, <https://doi.org/10.1016/j.cej.2020.126989>.
- [38] C. Barquín, M.J. Rivero, I. Ortiz, Shedding light on the performance of magnetically recoverable TiO₂/Fe₃O₄/GO-5 photocatalyst. Degradation of S-metolachlor as case study, *Chemosphere* 307 (2022) 135991, <https://doi.org/10.1016/j.chemosphere.2022.135991>.
- [39] G. Grause, M.F. Chien, C. Inoue, Changes during the weathering of polyolefins, *Polym. Degrad. Stab.* 181 (2020) 109364, <https://doi.org/10.1016/j.polymdegradstab.2020.109364>.
- [40] S. Lv, Q. Wang, Y. Li, L. Gu, R. Hu, Z. Chen, Z. Shao, Biodegradation of polystyrene (PS) and polypropylene (PP) by deep-sea psychrophilic bacteria of *Pseudoalteromonas* in accompany with simultaneous release of microplastics and nanoplastics, *Sci. Total Environ.* 948 (2024) 174857, <https://doi.org/10.1016/j.scitotenv.2024.174857>.
- [41] Y. Jang, I. Nyamjav, H.R. Kim, D.E. Suh, N. Park, Y.E. Lee, S. Lee, Identification of plastic-degrading bacteria in the human gut, *Sci. Total Environ.* 929 (2024) 172775, <https://doi.org/10.1016/j.scitotenv.2024.172775>.
- [42] X. Gu, L. Li, Y. Wu, W. Dong, Enhancement of microplastics degradation with MIL-101 modified BiOI photocatalyst under light and dark alternated system, *J. Environ. Chem. Eng.* 12 (2024) 112958, <https://doi.org/10.1016/j.jece.2024.112958>.
- [43] X. Chen, Y. Yue, Z. Wang, J. Sun, S. Dong, Co-existing inorganic anions influenced the Norrish I and Norrish II type photoaging mechanism of biodegradable microplastics, *Sci. Total Environ.* 925 (2024) 171756, <https://doi.org/10.1016/j.scitotenv.2024.171756>.
- [44] J. Fischer, G.M. Wallner, A. Pieber, Spectroscopical investigation of ski base materials, *Macromol. Symp.* 265 (2008) 28–36, <https://doi.org/10.1002/masy.200850504>.
- [45] M. Fadda, A. Sacco, K. Altmann, D. Ciornii, F. Milczewski, M.A. Bañares, R. Portela, A.M. Giovannozzi, A.M. Rossi, Tracking nanoplastics in drinking water: a new frontier with the combination of dielectrophoresis and Raman spectroscopy, *Microplast. Nanoplast.* 5 (2025) 24, <https://doi.org/10.1186/s43591-025-00131-y>.
- [46] M. Roškaric, G. Žerjav, J. Zavašnik, A. Pintar, The influence of synthesis conditions on the visible-light triggered photocatalytic activity of g-C₃N₄/TiO₂ composites used in AOPs, *J. Environ. Chem. Eng.* 10 (2022) 107656, <https://doi.org/10.1016/j.je.2022.107656>.
- [47] F. Parrino, A. Gottuso, L. Viganò, P. Mariani, I. Villa, F. Cova, E. Callone, S. Dirè, L. Palmisano, M. Stredansky, M. D'Arienzo, Singlet oxygen photocatalytic generation by silanized TiO₂ nanoparticles, *Angew. Chem. Int. Ed.* 64 (2024) e202414445, <https://doi.org/10.1002/anie.202414445>.
- [48] M. Adeel, C.F. Grasel Frois, I. Berruti, C. Sirtori, S. Malato, L. Rizzo, Activation of peroxymonosulfate by(sunlight)FeCl₃-modified biochar for efficient degradation of contaminants of emerging concern: comparison with H₂O₂ and effect of microplastics, *Chem. Eng. J.* 507 (2025) 160782, <https://doi.org/10.1016/j.cej.2025.160782>.
- [49] Q. Fatima, A.A. Haidry, H. Zhang, A. El Jery, M. Aldridery, A critical review on advancement and challenges in using TiO₂ as electron transport layer for perovskite solar cell, *Mater Today Sustain* 27 (2024) 100857–100866, <https://doi.org/10.1016/j.mtsust.2024.100857>.

- [50] L.A. Ningsih, P.Y. Lu, S. Ashimura, M. Yoshida, W.C. Chen, Y.C. Chiu, C. Hu, Highly effective photocatalytic degradation of plastic film (LDPE) using ruthenium-incorporated g-C₃N₄ via the Norrish mechanism, *Chem. Eng. J.* 480 (2024) 148089–148098, <https://doi.org/10.1016/j.cej.2023.148089>.
- [51] T.S. Tofa, K.L. Kunjali, S. Paul, J. Dutta, Visible light photocatalytic degradation of microplastic residues with zinc oxide nanorods, *Environ. Chem. Lett.* 17 (2019) 1341–1346, <https://doi.org/10.1007/s10311-019-00859-z>.
- [52] B. Gewert, M.M. Plassmann, M. Macleod, Pathways for degradation of plastic polymers floating in the marine environment, *Environ. Sci.: Processes Impacts* 17 (2015) 1513–1521, <https://doi.org/10.1039/c5em00207a>.
- [53] Q. Guo, D. Wei, C. Zhao, C. Wang, H. Ma, Y. Du, Physical UV-blocker TiO₂ nanocomposites elevated toxicity of chemical sunscreen BP-1 under UV irradiation, *Chem. Eng. J.* 469 (2023) 143899–143908, <https://doi.org/10.1016/j.cej.2023.143899>.
- [54] Á.D. Virág, C. Tóth, K. Molnár, Photodegradation of polylactic acid: characterisation of glassy and melt behaviour as a function of molecular weight, *Int. J. Biol. Macromol.* 252 (2023) 126336–126349, <https://doi.org/10.1016/j.ijbiomac.2023.126336>.
- [55] S. Therias, J.F. Larché, P.O. Bussière, J.L. Gardette, M. Murariu, P. Dubois, Photochemical behavior of polylactide/ZnO nanocomposite films, *Biomacromolecules* 13 (2012) 3283–3291, <https://doi.org/10.1021/bm301071w>.
- [56] J.A.F. Batista, J. Mendes, W.E. Moretto, M.S. Quadro, J.H.Z. dos Santos, C.C. de Escobar, Sunlight removal of diclofenac using g-C₃N₄, g-C₃N₄/Cl, g-C₃N₄/Nb₂O₅ and g-C₃N₄/TiO₂ photocatalysts, *J. Environ. Chem. Eng.* 12 (2024) 113016, <https://doi.org/10.1016/j.jece.2024.113016>.
- [57] A.L. Garcia-Costa, T.I.A. Gouveia, M.F.R. Pereira, A.M.T. Silva, L.M. Madeira, A. Alves, M.S.F. Santos, Intensification strategies for cytostatics degradation by ozone-based processes in aqueous phase, *J. Hazard. Mater.* 440 (2022) 129743, <https://doi.org/10.1016/j.jhazmat.2022.129743>.
- [58] C. Barquín, M.J. Rivero, I. Ortiz, Revealing the role of individual components in the high performance photocatalytic mineralization of mixtures of organohalogen pollutants, *J. Environ. Chem. Eng.* 12 (2024) 114572, <https://doi.org/10.1016/j.jece.2024.114572>.